ELSEVIER

Journal of Nuclear Materials 249 (1997) 77–86

journal of nuclear materials

A molecular dynamics study of temperature effects on defect production by displacement cascades in α-iron

F. Gao [a], D.J. Bacon [a,*], P.E.J. Flewitt [b], T.A. Lewis [b]

[a] *Department of Materials Science and Engineering, University of Liverpool, Liverpool L69 3BX, UK*
[b] *Technology & Central Engineering Division, Magnox Electric plc, Berkeley, Gloucestershire GL13 9PB, UK*

Received 4 February 1997; accepted 20 May 1997

Abstract

Assessment of the hardening and embrittlement of pressure vessel steels and welds as a function of neutron dose uses trend curves derived from surveillance specimens. For some materials in the UK typical of those used in older plant, these curves incorporate an empirical factor to describe the temperature-dependence of matrix hardening. In the present work, molecular dynamics (MD) simulations have been used to obtain detailed information on defect number and arrangement produced in the primary cascade state of radiation damage as functions of irradiation temperature, T_{irr}, in α-iron. To allow for heat dissipation during the thermal spike phase, the continuum treatment of heat conduction was used to adjust the temperature of the boundary atoms in MD throughout the cascade process. The continuum parameters were calibrated to match those of the atomic structure. This new hybrid model allows for the variability in form between one cascade and another and has been applied to defect generation by cascades of either 2 or 5 keV at 100 K, 400 K, 600 K and 900 K. The effect of T_{irr} on the production of Frenkel pairs is small but statistically significant: the total number decreases by about 20–30% as T_{irr} increases from 100 K to 900 K. The decrease is smaller than would be consistent with the factor in the trend curves, implying that most of the observed temperature dependence arises from postcascade processes. © 1997 Elsevier Science B.V.

1. Introduction

Analysis of several experiments on plate steels used in older nuclear power plant in the UK has permitted the temperature dependence of matrix hardening to be defined by the simple empirical factor

$$F_T = 1.869 - 4.57 \times 10^{-3} T, \quad (1)$$

where T is the irradiation temperature in °C [1]. The aim of the present work is to investigate, using computer simulation, to what extent this dependence is influenced by the primary damage production in the initial cascade process (as opposed to mechanisms in the postcascade evolution). Atomic-scale computer simulation based on molecular dynamics (MD) has been found to be a powerful method for investigating the mechanisms and scale of defect production in the radiation damage in metals caused by displacement cascades. (For recent reviews of this area see Refs. [2–5]). Research using MD has confirmed many of the ideas proposed by the early workers in the field (e.g., [6]) that a cascade proceeds initially by a ballistic phase, in which many atoms are displaced from their lattice sites, followed by a thermal-spike phase, in which the kinetic and potential components of the energy come to equilibrium as most atoms return to lattice sites and the cascade zone cools to the ambient temperature of the metal.

Computer modelling has put flesh on this skeletal description by showing that the disorder produced in the hot core during the thermal spike is akin to melting, albeit with a very short life of only a few ps. Most self-interstitial atoms (SIAs) are formed at the periphery of this zone by their failure to return to empty lattice sites, and the vacan-

* Corresponding author. E-mail: djbacon@liv.ac.uk.

PII S0022-3115(97)00178-5

cies are thus formed within the hot, disordered core as it cools. MD simulations have also shown that the production efficiency of Frenkel defects, i.e., vacancy-SIA pairs, is considerably smaller than the predicted value of the conventional NRT equation due to Norgett et al. [7] derived from the original hard-sphere collision model of Kinchin and Pease [8]. The NRT estimate for the number, N_F, of Frenkel pairs produced by a primary knock-on atom (PKA) with a damage energy E_p is

$$N_{NRT} = 0.8E_p/2E_d, \quad (2)$$

where E_d is the spatially-averaged threshold displacement energy. MD simulations for all metals reveal a value of N_F of only 20 to 40% of N_{NRT} for E_p values above about 1 to 2 keV. There is experimental evidence to support this reduced efficiency of the cascade process (e.g., [9,10]).

Another feature revealed by computer modelling is the extent to which defects actually cluster during the cascade phases. It has long been known from ion irradiations of TEM foils that a vacancy dislocation loop can form by vacancy clustering and collapse in the cascade core before the end of the thermal spike [11], but the simulations have shown that SIA clustering is also a feature of the primary damage state. Again, there is experimental evidence to support this (e.g., [12]) and it is believed to affect the way these defects contribute to the evolution of microstructure during subsequent diffusional processes in the material (e.g., [13]).

One limitation of much modelling to date is that the MD block has been usually taken to be adiabatic and, thus, the dissipation of this heat into the surrounding material (at the ambient temperature) was not accounted for correctly. In the case of cascades, approximately half the PKA energy is converted to kinetic energy distributed over the lattice by the end of the thermal spike, and the number of atoms in the MD block used for the simulations was such that the increase in block temperature was typically 200 to 300 K. This heating is sufficient to affect the mobility of SIAs in further continuation of the MD, since they can diffuse in most metals over the time period at the temperatures created: this is not an issue for the vacancies, which have a higher migration energy than SIAs.

Previous studies of the effect of lattice temperature on primary defect production in cascades have simply simulated cascades in MD blocks initially equilibrated at the chosen temperature [14,15]. They have indicated that for both iron and copper the N_F value and the level of SIA clustering may depend on the irradiation temperature, but the lack of a suitable treatment of thermal-spike cooling leaves room for uncertainty in the trends found. The present work was undertaken to rectify this for the metal α-iron and to obtain data for N_F and SIA clustering over the temperature range 100 to 900 K. To do this, we have developed a new treatment of the boundary atoms of the MD crystal, such that they lose or gain energy as though they were effectively in an infinite medium. This approach and its validation are described in Sections 2 and 3 and application of it to temperature effects on defect production in cascades in α-iron is presented in Section 4. The results are discussed in Section 5 and lead to the conclusion that most of the observed temperature-dependence of matrix damage does not arise during the formation of the primary damage state created by cascades.

2. Method

2.1. Basic idea

The hybrid model is shown in schematic form in Fig. 1, where the MD block is embedded in a continuum, which we call the thermal block. In order to extract heat from the MD block, the continuum and atomic spaces are partitioned into supercells at some initial time, t_0. There is a one-to-one correspondence between the supercells of the

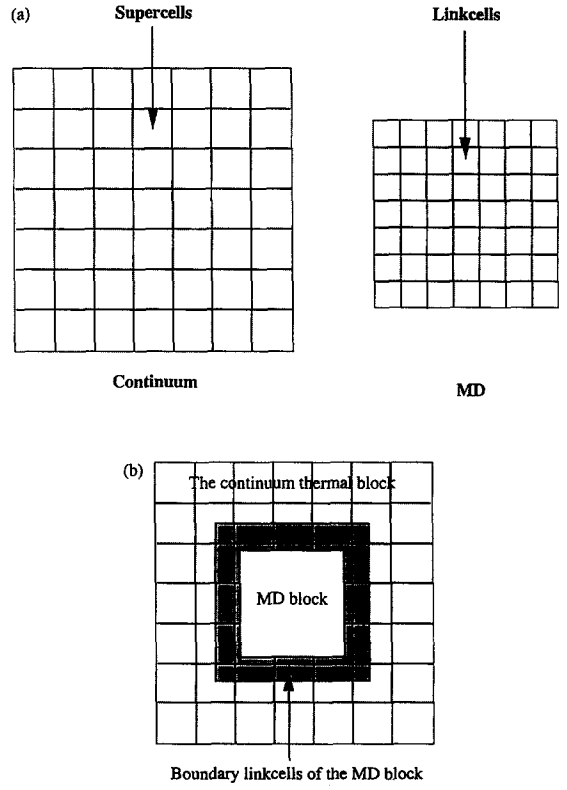

Fig. 1. Schematic illustration of the principle behind the method adopted here. (a) Calculations based on the MD atomic block and a larger continuum block with the same thermal conductivity are run in parallel. (b) The velocity of the boundary atoms of the MD block is adjusted to match the temperature distribution of the continuum.

two media at this time and the supercell size is sufficiently large for each cell to contain hundreds of atoms in the MD block. In this way, the temperature of a cell can be meaningfully defined in terms of the kinetic energy of its atoms. Thereafter, the supercell structure plays no part in the MD calculation, but is used to calculate the temperature distribution within the supercells of the continuum model at each MD timestep by the approach described by Caro et al. [16] (see next Section 2.2). Thus, the continuum and MD iterations run in parallel, but at each timestep the velocity of atoms in the boundary region of the MD block is scaled so that the temperature distribution in this region matches that of the continuum supercells with which it coincides (see Section 2.4). Since the continuum block can be made many times larger than the MD block, the heat transfer into or out of the latter follows that of a much bigger system.

2.2. Heat propagation in the continuum model

The equation of heat conduction in an isotropic, uniform medium with thermal conductivity κ and density ρ is

$$\frac{\partial T}{\partial t} = \nabla\{(\kappa/\rho)\nabla T\}, \tag{3}$$

where T is the temperature and t the time. We can write a discretized version of Eq. (3) in a simple cubic partitioning of the space into cells of linear dimension a:

$$\begin{aligned} T(\boldsymbol{r}, t+\Delta t) &= (\kappa\Delta t/\rho a^2)\{T(x+a, y, z, t) \\ &\quad + T(x-a, y, z, t) + T(x, y+a, z, t) \\ &\quad + T(x, y-a, z, t) + T(x, y, z+a, t) \\ &\quad + T(x, y, z-a, t) + [(\rho a^2/\kappa\Delta t) - 6]T(\boldsymbol{r}, t)\}, \end{aligned} \tag{4}$$

where ρ and κ may be functions of T and therefore of $\boldsymbol{r}$ and t. However, if we take spatial and temporal averages of these quantities and choose $\Delta t'$ such that

$$\Delta t' = (\rho a^2/\kappa), \tag{5}$$

then Eq. (4) takes the form of a simple average over nearest-neighbour cells, as used by Caro et al. [16] and Kapinos and Bacon [17], for example, to investigate the evolution of the thermal spike of cascades in the continuum approximation. It is easily generalised to anisotropic media, such as the HCP metals (Gao and Bacon, unpublished), where $\Delta t'$ may be different in the different crystallographic directions. In the present method, we take Δt to be the timestep in MD and hence have to determine the $\Delta t'$ that corresponds to the actual heat conduction in the MD model.

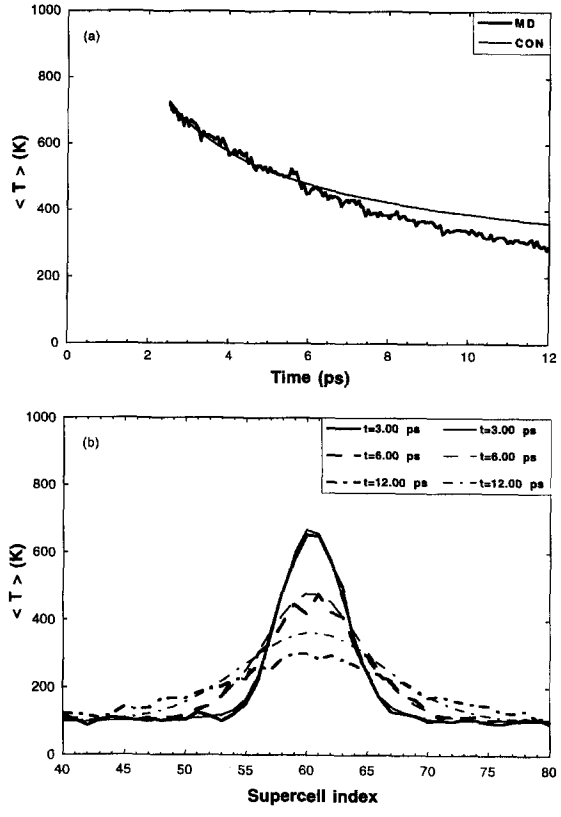

Fig. 2. (a) The temperature of the central cell as a function of time for one-dimensional heat flow and (b) the temperature distribution along the direction of heat flow at different times. The MD results are shown by bold lines, the continuum values by thin lines.

2.3. Determining the thermal conductivity

In order to determine the thermal conductivity, or equivalently $\Delta t'$, to be used in the continuum approximation of the real atomic system, we have used an elongated MD block of size $6a_0 \times 6a_0 \times 252a_0$ (= 18144 atoms for α-Fe), where a_0 is the lattice parameter. Periodic boundary conditions were imposed in all three directions. The crystal was first equilibrated at 100 K for 5 ps. To simulate one-dimensional heat transfer in this system, a Gaussian profile of temperature was then introduced into the central region of the crystal via the atomic velocities and the block was equilibrated for a further 3 ps to establish the phonon modes. At this time, the block was divided into supercells of size $6a_0 \times 6a_0 \times 6a_0$, each containing 432 atoms, and the temperature in each supercell was calculated to give the initial distribution of temperature for the continuum model. Eq. (5) was then solved for several hundred timesteps and the value of $\Delta t'$ was determined from the condition that the temperature distribution calculated by the continuum model was approximately the same as that simulated by MD over a period of 10–20 ps.

Good agreement was found for $\Delta t' = 0.651$ ps, as seen in Fig. 2(a) and (b), which show the temperature of the central cell as a function of time and the temperature profile of the central region at different times, as calculated by MD and the continuum model with $\Delta t'$ as given above. Better agreement could be obtained with a temperature-dependent κ, i.e., $\Delta t'$ should be smaller at low temperature, but this was not judged to be necessary for the present work. The value of 0.651 ps for $\Delta t'$ compares with 0.136 ps using the κ and ρ values for metallic iron and $a = 6a_0$ in Eq. (5). This difference is expected because the electronic contribution to κ is neglected in the MD model. It also shows that choice of the smaller value of $\Delta t'$ would be inappropriate for the heat spike of concern because the electrons can not come to equilibrium with the phonons in this time.

2.4. Temperature scaling

For a simulation using the new MD/continuum hybrid model, the MD and continuum calculations are run in parallel with timestep Δt. The initial temperature distribution for the continuum model is determined from the temperature of the supercells of the MD block at a suitable time and the evolution of the temperature is calculated from Eq. (5). The velocity of atoms in the linkcells at the boundary of the block is scaled at each timestep so that the temperature of each link cell matches that calculated for the supercell that contains it in the continuum approximation, i.e., the velocity of each atom is scaled by the formula

$$v_{\text{new}} = v_{\text{old}}(T_{\text{CON}}/T_{\text{MD}})^{1/2}, \tag{6}$$

where T_{CON} is the temperature calculated by the continuum model and T_{MD} the temperature by MD.

3. Testing the model

3.1. One-dimensional heat flow

A one-dimensional MD block of size of $6a_0 \times 6a_0 \times 95a_0$ and containing 6912 atoms was used to simulate the evolution of the Gaussian temperature distribution considered in Section 2.3. Periodic boundary conditions were imposed across all faces, but the temperature of the boundary linkcells along the longitudinal axis of the crystal was scaled by the distribution calculated by the continuum model, as described above. Fig. 3(a) shows the temperature in the central cell calculated by this hybrid method and that given by the much larger MD cell in Section 2.3 and Fig. 3(b) presents the axial temperature distribution in the two simulations. It can be seen that the temperature calculated by two methods is in good agreement.

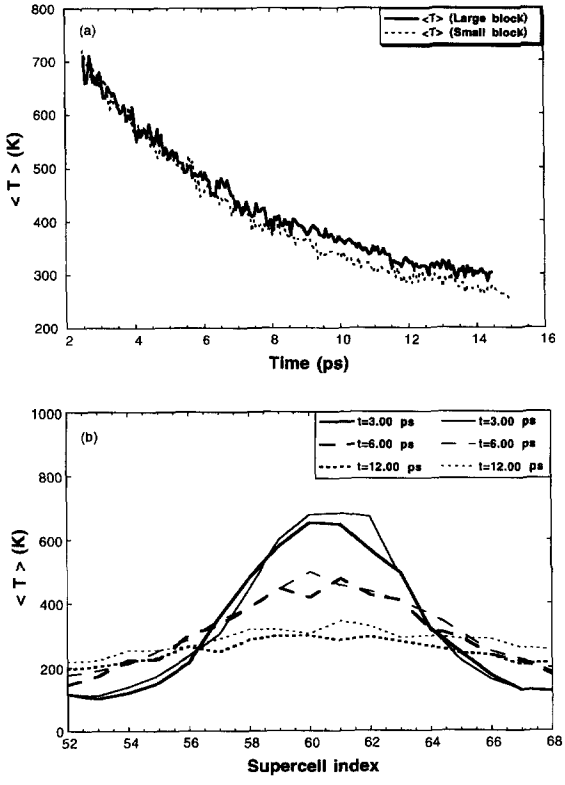

Fig. 3. (a) The temperature of the central cell as a function of time for one-dimensional heat flow and (b) the temperature distribution along the direction of heat flow at different times. The bold lines are those for the large MD block (Fig. 2) and the thin lines are for the hybrid model using a smaller MD block.

3.2. Three-dimensional heat flow

In the three-dimensional case, a large MD block of size $62a_0 \times 62a_0 \times 62a_0$ (containing 476 656 atoms) was first used to mimic the temperature evolution due to a spherical heat spike in an infinite medium. It was first equilibrated at 100 K for 3 ps and then a heat spike with Gaussian radial profile of temperature with a maximum of 1000 K was initiated in the centre of a crystal by applying a suitable distribution of kinetic energy to the atoms of the central seven shells of thickness $2a_0$. The temperature of the central cell and the radial temperature profile at different times are shown in Fig. 4(a) and (b), respectively.

A smaller MD crystal of size $28a_0 \times 28a_0 \times 28a_0$ (containing 43 904 atoms) was then used to simulate the same heat spike, but heat was extracted from the boundary link cells using the new scheme outlined in Section 2. The temperature of the central cell and the radial temperature profile at different times are also plotted in Fig. 4(a) and (b) and it can be seen that they are in good agreement with those calculated in the much bigger block. This demonstrates that the hybrid model can be used to enable a

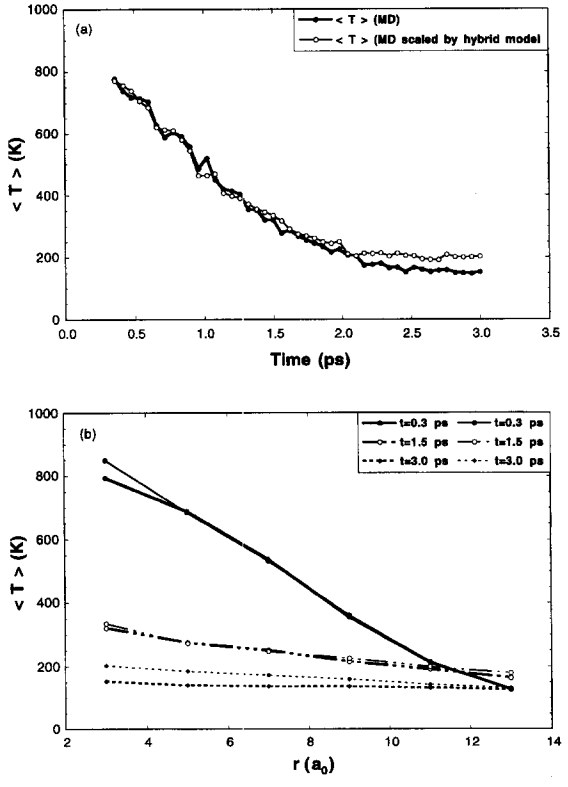

Fig. 4. (a) The temperature of the central cell as a function of time for three-dimensional heat flow and (b) the radial temperature distribution in spherical shells at different times. The results for a large MD block of 476656 atoms are shown by bold lines, those for a small block of 43904 atoms in the hybrid model are shown by thin lines.

relatively small MD crystal to mimic the temperature transfer in an infinite medium.

4. Displacement cascades in α-iron

4.1. Method

The MD program used for the cascade simulations was that used in previous work in this laboratory [14] and was a development of the MOLDY code [18]. It uses a link-cell method to generate neighbour tables for interactions between atoms and the size of a link cell is just a little larger than the range of the interatomic potential. The link-cell structure provides a natural framework for the boundary damping employed here, but is not a requirement for the successful implementation of the model. Calculations were performed at constant pressure and periodic boundary conditions were employed.

The many-body interatomic potential for α-Fe derived by Finnis and Sinclair [19], as modified by Calder and Bacon [14] for displacement damage modelling, was used for the simulations. It has the advantage that the previous cascade data for α-iron obtained in Refs. [14,15,20] used the same potential and can be compared directly. The crystal size was 54000 atoms($\equiv(30a_0)^3$) and 93312 atoms($\equiv(36a_0)^3$) for 2 and 5 keV, respectively.

To simulate a cascade, a block was first equilibrated for at least 10 ps at one of the specified temperatures, T_{irr}, of 100 K, 400 K, 600 K and 900 K, so that when the PKA event was initiated, the equilibrium phonon modes were already established. A cascade was started by imparting a kinetic energy E_{p} of either 2 or 5 keV to one atom, i.e., the PKA, following which the crystal was allowed to evolve for typically 1500 timesteps (~ 15 ps). In order to avoid channelling by the PKA, the high-index direction ⟨135⟩ was used for its initial recoil. For each T_{irr}, we ran four simulations at 2 keV and eight at 5 keV in order to generate meaningful cascade statistics.

At the end of the ballistically-induced displacement phase of a cascade, the number of temporarily displaced atoms reaches a maximum. This occurs after 0.1 to 1.0 ps, depending on E_{p}. Beyond this time, t_{peak}, the velocity of atoms in the core has an approximately Maxwellian distribution and the thermal energy generated by the PKA is gradually dissipated into the remainder of the crystal. Accordingly, the temperature in each supercell of the MD block was calculated at this time to give the initial distribution of temperature for the continuum model. From this point on, the continuum model was used to scale the temperature on the boundaries of the MD block, as described in Section 2, and scaling was continued until the end of the thermal-spike phase and beyond. The size of the continuum model was taken to be three times that of the MD block.

4.2. Generation of cascades

Fig. 5(a) shows the variation of the lattice temperature, $\langle T\rangle$, averaged over the MD block with time for two 5 keV cascades at 100 K and two at 600 K, where the cascades were simulated either with or without scaling at the boundaries. For both temperature conditions the average lattice temperature for the cascades with boundary scaling reduces towards the ambient temperature as heat within the cascade core is dissipated and reaches within about 50° of T_{irr} after about 6 ps. The lattice temperature $\langle T\rangle$ without boundary scaling also decreases with increasing time after t_{peak}, but with quite different behaviour. It declines slowly (because of the approximation involved in integrating the equations of motion), but is considerably higher than that of the block with appropriate boundary conditions, even after 12 ps. It can be seen that the new hybrid model gives a more realistic description in terms of the role of lattice conductivity in the evolution of cascades.

The variation in the number, N_{d}, of displaced atoms with time for the same cascade simulations is shown in

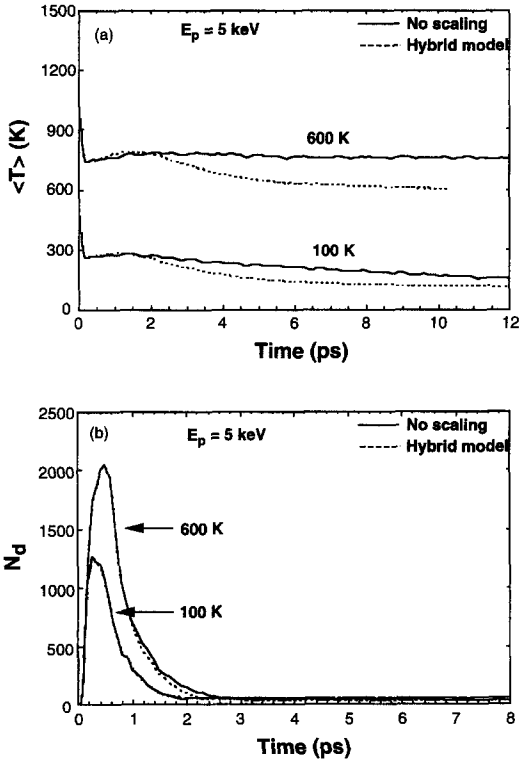

Fig. 5. (a) The average temperature and (b) the number of displaced atoms for 5 keV cascades in the MD block initially at 100 K and 600 K. Results for a block without boundary scaling are shown by continuous lines, those for a block using the hybrid model are shown by broken lines.

Fig. 5(b). As in the description by Calder and Bacon [14], a 'displaced' atom is defined as one that does not lie within 0.3 a_0 of a lattice site and, conversely, any site that does not have an atom within 0.3 a_0 of it is defined as a vacant site. During the collisional phase of a cascade, the number of displaced atoms, N_d, increases with time and achieves a maximum at time t_{peak}. As described above, the continuum model was initiated at this time. The form of, and effect of T_{irr} on, the N_d vs. time plots are similar to those reported in [14]. After t_{peak}, the values of N_d in the hybrid model for both temperatures are similar to those without heat extraction, i.e., they decline during subsequent recombination with very similar behaviour. The timescale for this reduction in N_d is essentially independent of the boundary condition. However, a feature not apparent in Fig. 5(b) is that number of stable Frenkel pairs, N_F, created at the end of the cascade process is actually slightly different in the two modelling procedures. N_F at T_{irr} = 100 K is 27 with boundary scaling and 24 without and at 600 K is 18 and 16, respectively. We now consider whether these differences are statistically significant.

4.3. Temperature analysis of cascades

The plots of Fig. 6(a) and (b) are the radial temperature profile at different times during the thermal spike phase for a 5 keV cascade at T_{irr} = 100 and 600 K. The temperature shown is the mean in spherical shells of thickness either $0.36a_0$ or $0.54a_0$ for 100 and 600 K, respectively, and centred on the 'centre of gravity' of the displaced atoms at the time t_{peak}. The core region in the two cascades attains a very high effective temperature and using this data we have analysed the maximum size of the spherical zone within which the effective temperature exceeds the melting temperature, T_m(= 1809 K).

The radius, R_{melt}, defined in this way is plotted as a function of time in Fig. 7. It can be seen that the region of material where the temperature is in excess of T_m is bigger for 600 K than for 100 K, and the time for it to shrink to a given size is longer, i.e., the lifetime of the thermal spike at 600 K is longer than that at 100 K for the same PKA energy. This is also clear from Fig. 8 in which the temperature in the sphere with radius set equal to the initial value

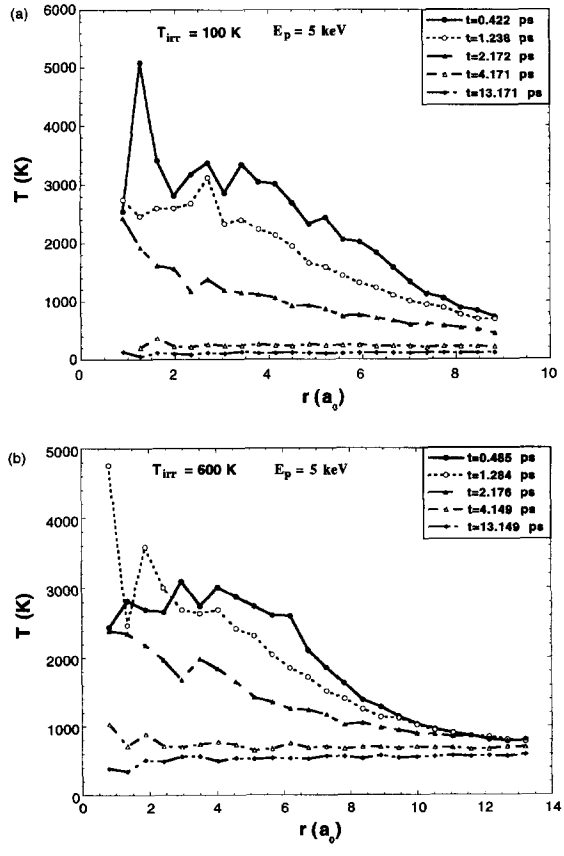

Fig. 6. The variation of the mean temperature in spherical shells of thickness (a) $0.36a_0$ for 100 K and (b) $0.54a_0$ for 600 K at the different times.

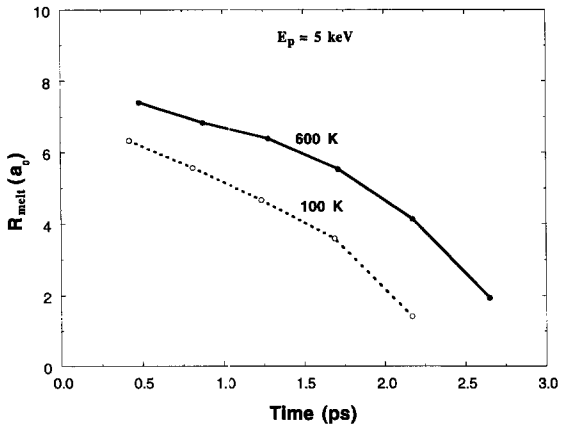

Fig. 7. Data for R_{melt} defined in the text as a function of time for T_{irr} = 100 K and 600 K.

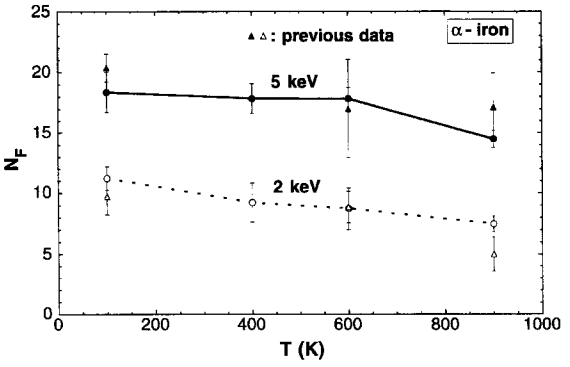

Fig. 9. Data for the number of Frenkel pairs produced per cascade as a function of PKA energy and initial crystal temperature. (○) Data obtained using the boundary treatment developed here; (▲) values obtained previously in [14,15] when thermal conduction out of the model was not allowed.

of R_{melt}, $T(R_{melt}(t_{peak}))$, is plotted as a function of the time. The initial temperature is about 2480 K for both 100 and 600 K, but the decrease of the temperature at 100 K is faster than that for 600 K. It is also clear from this plot that the time required to arrive at a given temperature for T_{irr} = 600 is longer than that for 100 K.

4.4. Point defect production and clustering

The data for the final number Frenkel pairs, N_F, at the end of the simulations for 2 and 5 keV cascades using the new hybrid treatment are plotted as a function of temperature in Fig. 9, together with data obtained by Calder and Bacon [14] and Phythian et al. [15] using conventional MD. (Values of N_F for 2 keV cascades at 900 K were not determined in the earlier studies and have been computed here for completeness using the original boundary conditions). The line joining the points denotes the means and the bars indicate the standard error.

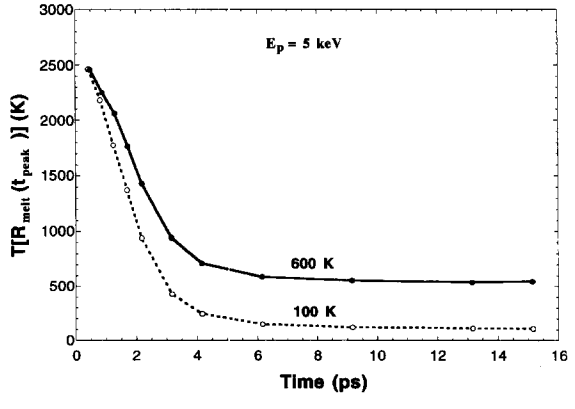

Fig. 8. The variation with time of the temperature in the sphere of radius R_{melt} at t_{peak} for T_{irr} = 100 K and 600 K.

The number of Frenkel pairs decreases with increasing temperature. This is due to the increase in the lifetime of the thermal spike (Figs. 7 and 8), which allows more defect motion to take place before cooling and hence leads to more SIA-vacancy recombination. Comparing the sets of data for 2 and 5 keV from [14] and [15] with those obtained in the present work, it is seen that the numbers of Frenkel pairs are in reasonable agreement, except for the data for cascades at 900 K. This demonstrates that the results simulated by MD without damping the boundaries are not strongly in error. The difference in cascade cooling rate due to the more accurate simulation of heat conduction through the lattice ion system seems to have little effect on N_F. However, this would need to be confirmed for higher energy cascades where the lifetime of the thermal spike is much longer than that in low energy cascades.

If the matrix embrittlement is assumed to be directly related to the number of Frenkel pairs produced in the cascade process, then the data of Fig. 9 is consistent with dF_T/dT values (see Eq. (1)) of approximately -0.2×10^{-3} and -0.5×10^{-3} °C^{-1} for the 2 and 5 keV cascades, respectively. Both values are significantly less than the empirical value of -4.57×10^{-3} °C^{-1} indicated by Eq. (1) for a narrower temperature range, thereby suggesting that either the observed dependence does not arise from temperature effects on the primary damage state created by cascades or that N_F may not be the controlling parameter. For example, the formation of clusters may be influential.

An important feature in the evolution of radiation damage is the tendency of defects to cluster in cascades. As explained by Singh and Evans [13], for example, clustering by the end of the cascade process affects defect behaviour and microstructural changes in subsequent evolution of the damage. To consider SIA clustering here, we follow the

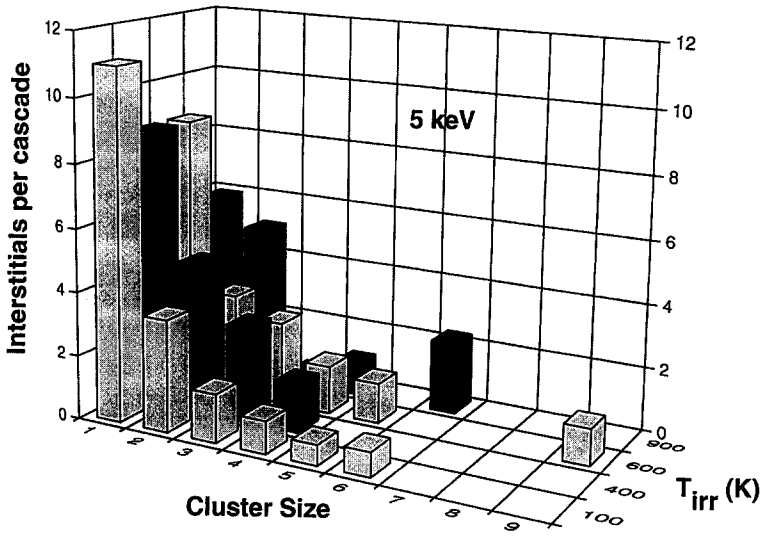

Fig. 10. Data for the number of interstitials per cascade in clusters of given size for each initial crystal temperature for PKA energy of 5 keV.

method in [14,15] by defining an interstitial cluster such that within it, every defect has at least one nearest-neighbour SIA. Data for the cluster distribution of interstitial defects at the end of the 5 keV cascade process, averaged over all the cascades, are plotted in the form of an histogram in Fig. 10. The number and size of SIA clusters steadily increase with T_{irr}, so that at 900 K an appreciable fraction of the SIAs are produced in cluster form, i.e., 69 out of the total of 116 SIAs found in cascades were in clusters of two or more, compared with 59 out of 147 at 100 K. The largest cluster size was 9 for 5 keV cascades and 4 for 2 keV, which is very similar to those found in α-Fe by using the MD model with no damping [15]. However, the tendency for interstitial clustering to change with the lattice temperature is different in the two sets of simulations. This can be illustrated as follows.

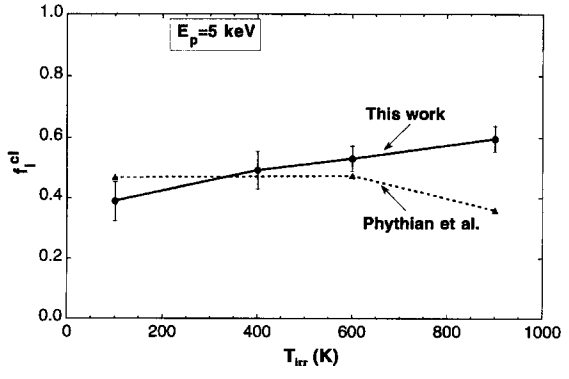

Fig. 11. Variation of the interstitial clustering fraction as a function of initial lattice temperature for 5 keV cascades using data obtained in this work and by Phythian et al. [15].

The interstitial clustering fraction, f_i^{cl}, is defined to be the fraction of surviving interstitials found in clusters of size two or larger. It is an important factor in the rate theory model of damage evolution and was calculated for α-Fe and Cu using the conventional MD model by Phythian et al. [15]. It was found that f_i^{cl} in iron has little sensitivity on temperature between 100 and 600 K and then falls significantly by 900 K and a similar effect was found from the simulations of Cu using the same adiabatic boundary conditions [15]. The new hybrid model is able to simulate cascades in a lattice at the correct temperature throughout the thermal spike and should give more realistic results. The value of f_i^{cl} obtained using this model is shown as a function of the temperature T_{irr} for 5 keV cascades in Fig. 11, together with data from the earlier simulations. The points represent the mean values and the bars indicate the standard error. The current simulations show that the interstitial clustering fraction increases steadily with increasing T_{irr} over the whole temperature range considered. Thus, the T-dependence of Eq. (1) is not consistent with the dependence of clustering in the cascade process.

5. Discussion

An investigation using MD has been made of the effect of lattice temperature on the production of vacancies and interstitial atoms in the primary damage process associated with displacement cascades in α-iron. A method has been developed to overcome the deficiencies of some previous studies, wherein the MD crystal was treated as an adiabatic system and the heat generated by deposition of the kinetic

energy of the PKA was not extracted. Other investigations have used methods to damp the boundaries in the MD model by adding a dissipative force component to the equations of motion for the boundary atoms. Beeler [21] treated the boundaries with a formula based on an analogy of a damped, one-dimensional oscillator, and Erginsoy et al. [22] applied a constant force and a spring force on the boundary atoms to extract heat. King and Benedek [23] simply fixed the atoms of the boundary layers. Each of these methods modifies the integration schemes for position and velocity of the boundary atoms and the choice of the various force constants is not unequivocal, so that Laakkonen and Nieminen [24] employed another way to treat the boundary atoms. They calculated the kinetic energy of these atoms periodically. If it exceeded a given limit, the atomic velocity was scaled down to some low value but the direction of velocity was retained. In the studies of displacement cascades in copper by Diaz de la Rubia and Guinan [25] and Prönnecke at al. [26], the atoms in the boundary link cells were damped with a constant damping coefficient to match the expected overall rate of heat loss into a larger crystal, and the same cells were effectively linked to a thermal reservoir by applying a random force to each atom at each timestep such that the temperature can be controlled. The coupling with the thermal bath has no simple physical meaning, however.

The method employed here scales the velocity of the boundary atoms based on the continuum description of thermal conduction without changing their direction, and the thermal conductivity is determined to match that of the real atomic system. The calculation is fast, with almost no overhead on the MD computation and, in principle, can be used for a wide variety of boundary conditions and size of medium. Since the supercell array is only used in the MD block to determine temperatures at the initial time t_0, subsequent shape/volume changes in the MD model, such as occur in constant-pressure simulations, do not affect the continuum calculations. t_0 can be chosen as any convenient time when temperature can be determined from the atomic velocities. In the case of cascades, we use the temperature distribution at the time t_{peak}, corresponding to the cessation of the ballistic phase and the onset of the thermal spike phase, as the initial temperature distribution of the continuum. The initial temperature distribution of the continuum has the real form of the phenomenon under consideration. This is of possible importance for displacement cascades, where the deposition of energy in the ballistic phase can be irregular.

The role of electrons in the cascade process by electron–phonon coupling and heat conduction via the electron system was ignored in the present treatment. It may be important in iron [27,28] and, although electron–phonon coupling cannot be incorporated in conventional MD methods with any accuracy, the hybrid model developed here would allow both coupling (in the approximation employed by Finnis et al. [29]) and electronic conductivity (via adjustment to the continuum parameter $\Delta t'$) to be studied to a reasonable level of approximation.

The results presented in Section 4 for the time-dependence of the temperature in the cascade core show clearly that the lifetime of the thermal spike is longer for a given PKA energy at the higher lattice temperature T_{irr}. This effect results in a decrease in the production efficiency of Frenkel defects as T_{irr} increases because it allows for more efficient recombination of SIAs with vacant sites. It also permits a greater degree of SIA clustering in the primary damage state as T_{irr} increases and, again, this probably arises from the assistance given to SIA motion before the thermal spike ceases to play a role. These results form the most comprehensive and realistic set produced to date on temperature effects in cascades and, although they show that the overall scale of defect production found in previous simulations with conventional MD models did not contain a large error due to the approximation used, they do reveal some inconsistencies in the trends reported earlier. They demonstrate the need to incorporate heat transfer as accurately as possible when the quantitative details of irradiation temperature are of concern in the description of defect production.

The main aim of this work was to gain insight into whether the observed temperature-dependence of matrix hardening, characterised by the simple empirical factor F_T, is influenced by the effect of temperature on the cascade process itself or subsequent longer-term migration of defects. The number, N_F, of Frenkel pairs remaining at the end of the cascade has been shown to have a dependence about an order of magnitude less than that observed for hardening. It must be concluded that the observed temperature dependence arises during the evolution of the damage after the cascade process has ended.

6. Conclusions

(1) A modification of the standard MD method has been developed to investigate the number and arrangement of defects produced as a function of irradiation temperature in α-iron. This has been achieved by embedding the MD cell in an appropriate continuum. The accuracy of this has been demonstrated against the cooling of 1-D and 3-D models.

(2) The lifetime of the thermal spike is longer for higher irradiation temperature and it is believed that this factor accounts for most of the effects observed.

(3) The number of point defects produced in the cascade process is predicted to decrease with increasing irradiation temperature.

(4) The fraction of interstitials in clusters increases with increasing temperature, probably as a result of the longer thermal spike giving greater assistance to intracascade motion of these defects.

(5) Neither the variation of the number of point defects nor of the interstitial cluster fraction with irradiation tem-

perature is consistent with the empirical dependence of the factor F_T in Eq. (1).

Acknowledgements

This research was supported by a grant from the Engineering and Physical Sciences Research Council and financial assistance from Magnox Electric plc. The paper is published with the permission of the Director of Technology and Central Engineering of Magnox Electric plc.

References

[1] R.B. Jones, T.J. Williams, ASTM STP 1270 (1996) 569.
[2] T. Diaz de la Rubia, W.J. Phythian, J. Nucl. Mater. 191–194 (1992) 108.
[3] D.J. Bacon, T. Diaz de la Rubia, J. Nucl. Mater. 216 (1994) 275.
[4] D.J. Bacon, A.F. Calder, F. Gao, V.G. Kapinos, S.J. Wooding, Nucl. Instrum. Meth. B102 (1995) 37.
[5] D.J. Bacon, in: Computer Simulation in Materials Science, eds. H.O. Kirchner, L.P. Kubin and V. Pontikis (Kluwer Academic, Dortrecht, 1996) p. 189.
[6] A. Seeger, Proc. 2nd UN Conf. on Peaceful Uses of Atomic Energy, IAEA, Vienna, 1958, p. 250.
[7] M.J. Norgett, M.T. Robinson, I.M. Torrens, Nucl. Eng. Des. 33 (1975) 50.
[8] G.H. Kinchin, R.S. Pease, Rep. Prog. Phys. 18 (1955) 111.
[9] P. Jung, J. Nucl. Mater. 117 (1983) 70.
[10] J.H. Kinney, M.W. Guinan, Z.A. Munir, J. Nucl. Mater. 122&123 (1984) 1028.
[11] C.A. English, M.L. Jenkins, Mater. Sci. Forum 15–18 (1987) 1003.
[12] R. Rauch, J. Peisl, A. Schmalzbauer, G. Wallner, J. Nucl. Mater. 168 (1989) 101.
[13] B.N. Singh, J.H. Evans, J. Nucl. Mater. 226 (1995) 277.
[14] A.F. Calder, D.J. Bacon, J. Nucl. Mater. 207 (1993) 22.
[15] W.J. Phythian, A.J.E. Foreman, R.E. Stoller, D.J. Bacon, A.F. Calder, J. Nucl. Mater. 223 (1995) 245.
[16] M. Caro, A. Ardelea, A. Caro, J. Mater. Res. 5 (1990) 2652.
[17] V.G. Kapinos, D.J. Bacon, Phys. Rev. B52 (1995) 4029.
[18] M.W. Finnis, UKAEA Harwell Report, AERE R-13182, 1988.
[19] M.W. Finnis, J.E. Sinclair, Philos. Mag. A50 (1984) 45.
[20] F. Gao, D.J. Bacon, A.F. Calder, P.E.J. Flewitt, T.R. Lewis, J. Nucl. Mater. 230 (1996) 47.
[21] R. Beeler, Radiation Effects Computer Experiments (North-Holland, Amsterdam, 1983).
[22] C. Erginsoy, G.H. Vineyard, A. Englert, Phys. Rev. A133 (1964) 595.
[23] W.E. King, R. Benedek, J. Nucl. Mater. 117 (1983) 26.
[24] J. Laakkonen, R.M. Nieminen, Phys. Rev. B41 (1990) 3978.
[25] T. Diaz de la Rubia, M.W. Guinan, J. Nucl. Mater. 174 (1990) 151.
[26] S. Prönnecke, A. Caro, M. Victoria, T. Diaz de la Rubia, M.W. Guinan, J. Mater. Res. 6 (1991) 483.
[27] M.W. Finnis, in: Materials Modelling: From Theory to Technology (Institute of Physics, Bristol, 1992) p. 99.
[28] C.P. Flynn, R.S. Averback, Phys. Rev. B38 (1988) 7118.
[29] M.W. Finnis, P. Agnew, A.J.E. Foreman, Phys. Rev. B44 (1991) 567.